

Experimentally determining the exchange parameters of quasi-two-dimensional Heisenberg magnets

This article has been downloaded from IOPscience. Please scroll down to see the full text article.

2008 New J. Phys. 10 083025

(<http://iopscience.iop.org/1367-2630/10/8/083025>)

View [the table of contents for this issue](#), or go to the [journal homepage](#) for more

Download details:

IP Address: 129.169.10.56

The article was downloaded on 11/09/2010 at 19:20

Please note that [terms and conditions apply](#).

Experimentally determining the exchange parameters of quasi-two-dimensional Heisenberg magnets

P A Goddard^{1,7}, J Singleton², P Sengupta^{2,3}, R D McDonald²,
T Lancaster¹, S J Blundell¹, F L Pratt⁴, S Cox², N Harrison²,
J L Manson⁵, H I Southerland⁵ and J A Schlueter⁶

¹ Clarendon Laboratory, Department of Physics, University of Oxford,
Parks Road, Oxford OX1 3PU, UK

² National High Magnetic Field Laboratory, Los Alamos National Laboratory,
MS-E536, Los Alamos, NM 87545, USA

³ Theoretical Division, Los Alamos National Laboratory, Los Alamos,
NM 87545, USA

⁴ ISIS Facility, Rutherford Appleton Laboratory, Chilton, Oxfordshire,
OX11 0QX, UK

⁵ Department of Chemistry and Biochemistry, Eastern Washington University,
Cheney, WA 99004, USA

⁶ Materials Science Division, Argonne National Laboratory, Argonne,
IL 60439, USA

E-mail: p.goddard1@physics.ox.ac.uk

New Journal of Physics **10** (2008) 083025 (11pp)

Received 23 May 2008

Published 19 August 2008

Online at <http://www.njp.org/>

doi:10.1088/1367-2630/10/8/083025

Abstract. Though long-range magnetic order cannot occur at temperatures $T > 0$ in a perfect two-dimensional (2D) Heisenberg magnet, real quasi-2D materials will invariably possess nonzero inter-plane coupling J_{\perp} driving the system to order at elevated temperatures. This process can be studied using quantum Monte Carlo calculations. However, it is difficult to test the results of these calculations experimentally since for highly anisotropic materials in which the in-plane coupling is comparable with attainable magnetic fields J_{\perp} is necessarily very small and inaccessible directly. In addition, because of the large anisotropy, the Néel temperatures are low and difficult to determine from thermodynamic measurements. Here, we present an elegant method of assessing the calculations via two independent experimental probes: pulsed-field magnetization in fields of up to 85 T, and muon-spin rotation.

⁷ Author to whom any correspondence should be addressed.

We successfully demonstrate the application of this method for nine metal–organic Cu-based quasi-2D magnets with pyrazine (pyz) bridges. Our results suggest the superexchange efficiency of the $[\text{Cu}(\text{HF}_2)(\text{pyz})_2]\text{X}$ family of compounds (where X can be ClO_4 , BF_4 , PF_6 , SbF_6 and AsF_6) might be controlled by the tilting of the pyz molecule with respect to the 2D planes.

Contents

1. Introduction	2
2. Experimental details	3
3. Experimental results	4
4. Monte Carlo simulations of magnetization data	4
5. Comparisons of model and data	6
6. Systematic trends in the $[\text{Cu}(\text{HF}_2)(\text{pyz})_2]\text{X}$ family	8
7. Summary	10
Acknowledgments	10
References	11

1. Introduction

Systems that can be described by the $S = \frac{1}{2}$ two-dimensional (2D) square-lattice quantum Heisenberg antiferromagnet model [1]–[3] continue to attract considerable experimental [4, 5] and theoretical [6]–[9] attention. Recent impetus has been added to this field by suggestions that antiferromagnetic fluctuations from $S = \frac{1}{2}$ ions on a square lattice play a pivotal role in the mechanisms for superconductivity in the ‘high T_c ’ cuprates [3], [10]–[14] and other correlated-electron systems [15]; moreover, 2D Heisenberg magnets have been suggested as possible test-beds for processes applicable to quantum computation [4, 9].

Although long-range magnetic order cannot occur above $T = 0$ in a true 2D Heisenberg system [2, 16], real materials that contain planes approximating to 2D Heisenberg systems [2, 4, 17, 18] inevitably possess inter-plane coupling that can lead to a finite Néel temperature [4, 17, 19]. In this context, synthesis of coordination complexes containing ions such as Cu^{2+} , neutral bridging ligands [4] and coordinating anion molecules [17, 18] has proved fruitful in the production of a variety of 1D and 2D magnetic systems [17], [20]–[22]. The current paper describes high-field magnetization measurements on nine Cu-based (Cu^{2+} , $S = 1/2$) quasi-2D Heisenberg magnets that employ pyrazine (pyz) as a neutral bridging ligand [17, 18]⁸. The data show that the field (B)-dependent, low-temperature magnetization $M(B)$ shows a characteristic sharp ‘elbow’ feature at the transition to saturation, with a concave curvature at lower B . Monte Carlo evaluations of a 2D Heisenberg square lattice with an additional inter-plane exchange coupling energy J_{\perp} reproduce the data quantitatively; the degree of concavity depends on the effective dimensionality of the system, while the field at which the ‘elbow’ occurs is an accurate measure of the in-plane exchange energy J . Using these

⁸ Crystallographic data have been deposited with the Cambridge Crystallographic Data Centre (CCDC) No. 636104; 683410–683415. Copies of this information may be obtained free of charge from the Director, CCDC, 12 Union Road, Cambridge CB2-1EZ, UK. Fax: +44-1223-336033; <http://www.ccdc.cam.ac.uk/conts/retrieving.html>.

Table 1. The quasi-2D magnets studied in this work, along with their saturation fields B_c and g -factors (here pyz is pyrazine, pyo is pyridine-N-oxide). Data for oriented single crystals are indicated by B_{\parallel} (B parallel to 2D layers) and B_{\perp} (B perpendicular to 2D layers); other data are for powders. In the latter cases, an average g was evaluated from single-crystal electron paramagnetic resonance (EPR) data using standard formulae [25]. The in-plane exchange energy is calculated using equation (2); typical uncertainties in the values of J resulting from uncertainties in g and B_c are ± 0.1 K. Neél temperatures T_N were measured to ± 0.04 K using μ SR [22], apart from $\text{Cu}(\text{pyz})_2(\text{ReO}_4)_2$, where the transition was observed in heat capacity data (see footnote 8) (typical uncertainty ± 0.1 K). The anisotropy $|J_{\perp}/J|$ is calculated using equation (3). The magnetic properties of a number of other quasi-2D antiferromagnets based on copper–pyrazine coordination complexes can be found in [26].

Compound	B_c (T)	g	$ J $ (K)	T_N (K)	$ J_{\perp}/J $
$[\text{Cu}(\text{HF}_2)(\text{pyz})_2]\text{BF}_4$	18.0	2.13 ± 0.01	6.3	1.54	9×10^{-4}
$[\text{Cu}(\text{HF}_2)(\text{pyz})_2]\text{ClO}_4$ B_{\perp}	19.1	2.30 ± 0.01	7.3	1.94	2×10^{-3}
$[\text{Cu}(\text{HF}_2)(\text{pyz})_2]\text{ClO}_4$ B_{\parallel}	20.9	2.07 ± 0.01	7.2	1.94	2×10^{-3}
$[\text{Cu}(\text{HF}_2)(\text{pyz})_2]\text{PF}_6$	35.5	2.11 ± 0.01	12.4	4.31	1×10^{-2}
$[\text{Cu}(\text{HF}_2)(\text{pyz})_2]\text{SbF}_6$	37.6	2.14 ± 0.01	13.3	4.31	9×10^{-3}
$[\text{Cu}(\text{HF}_2)(\text{pyz})_2]\text{AsF}_6$	36.1	2.13 ± 0.01	12.8	4.34	1×10^{-2}
$[\text{Cu}(\text{pyo})_2(\text{pyz})_2](\text{ClO}_4)_2$ B_{\perp}	20.8	2.30 ± 0.01	7.9	< 2.0	$\lesssim 10^{-3}$
$[\text{Cu}(\text{pyo})_2(\text{pyz})_2](\text{ClO}_4)_2$ B_{\parallel}	22.2	2.07 ± 0.01	7.6	< 2.0	$\lesssim 10^{-3}$
$\text{CuF}_2(\text{pyz})(\text{H}_2\text{O})_2$ B_{\perp} ^a	28.8	2.42 ± 0.02	11.6	2.54	3×10^{-4}
$\text{CuF}_2(\text{pyz})(\text{H}_2\text{O})_2$ B_{\parallel} ^a	33.1	2.09 ± 0.01	11.5	2.54	4×10^{-4}
$\text{Cu}(\text{pyz})_2(\text{ReO}_4)_2$	42.7	2.13 ± 0.01	15.1	4.2	3×10^{-3}
$\text{Cu}(\text{pyz})_2(\text{H}_2\text{O})_2\text{Cr}_2\text{O}_7$	13.3	2.13 ± 0.01	4.7	< 1.6	$\lesssim 1 \times 10^{-2}$

^aAlthough $\text{CuF}_2(\text{pyz})(\text{H}_2\text{O})_2$ forms linear copper–pyrazine chains, EPR measurements on this compound have shown that the dominant superexchange pathway is through the hydrogen bonds between the water molecules and fluorine ions, and hence almost perpendicular to the chains. The result is a quasi-2D antiferromagnet on a square lattice [23, 24].

J values in conjunction with Neél temperatures deduced from muon-spin rotation (μ SR), it is then possible to gain a good estimate of the exchange anisotropy $|J_{\perp}/J|$ for all of the magnets.

Having established these findings using the whole range of compounds, we suggest that in magnets of the form $[\text{Cu}(\text{HF}_2)(\text{pyz})_2]\text{X}$, [18, 19] where X is a non-coordinating counterion, J and J_{\perp} may be influenced by the tilting of the pyz molecule with respect to the 2D planes.

2. Experimental details

The quasi-2D magnets studied in this work are listed in table 1. The samples are produced in single or polycrystalline form via aqueous chemical reaction between the appropriate CuX_2 salts and stoichiometric amounts of the ligands; further details are given in [18, 27] and footnote 8, where structural data derived from x-ray crystallography are also found. For some compounds, it was possible to grow crystals large enough to permit measurements with a single

orientated sample (table 1). In other cases, the materials were either polycrystalline or the crystals too small for accurate orientation; therefore, samples composed of many randomly orientated microcrystals, effectively powders were used. In addition to the characterization described in [18] (see footnote 8) sample g -factors were measured [28] using standard EPR techniques [25, 29].

The pulsed-field magnetization experiments used a 1.5 mm bore, 1.5 mm long, 1500-turn compensated-coil susceptometer, constructed from 50 gauge high-purity copper wire [30, 31]. When a sample is within the coil, the signal is $V \propto (dM/dt)$, where t is the time. Numerical integration is used to evaluate M [30]. The sample is mounted within a 1.3 mm diameter ampoule that can be moved in and out of the coil [30]. Accurate values of M are obtained by subtracting empty coil data from that measured under identical conditions with the sample present.

Fields were provided by the 65 T short-pulse and 100 T multi-shot magnets at NHMFL Los Alamos [32] and a 60 T short-pulse magnet at Oxford. The susceptometer was placed within a ^3He cryostat providing T s down to 0.4 K. B was measured by integrating the voltage induced in a ten-turn coil calibrated by observing the de Haas–van Alphen oscillations of the belly orbits of the copper coils of the susceptometer [31].

In cases where sufficient quantities of materials were available, Néel temperatures T_N were measured using the zero-field μSR technique described in [22] (see also [19, 27]). Muons are a useful probe of magnetic order in anisotropic spin systems, where more conventional measurement techniques often encounter several difficulties. These difficulties stem from the build-up of spin correlations at temperatures above T_N , which reduce the amount of entropy available to be ejected upon magnetic ordering (and hence reduce the response of the specific heat at T_N), and the quantum renormalization of the magnetic moment due to spin fluctuations (which hampers susceptibility and neutron measurements) [22]. In general, μSR measurements are unaffected by these issues and have been shown to be sensitive to magnetic order in several anisotropic molecular magnets [19, 22, 27]. Thus, μSR is vital for accurately determining the transition temperatures of the quasi-2D systems described here.

3. Experimental results

Typical $M(B)$ data are shown in figure 1; all compounds studied (table 1) behaved in a very similar fashion. At higher T , $M(B)$ is convex, showing a gradual approach to saturation at high B . However, as $T \rightarrow 0$, the $M(B)$ data become concave at lower B , with a sharp, ‘elbow’-like transition to a constant saturation magnetization M_{sat} at higher B ; no further changes in M occur to fields of 85 T with the current materials. We label the field at which the ‘elbow’ occurs B_c . As shown in figure 1(b), B_c depends on the crystal’s orientation in the field. However, in such cases, the M data become identical to within experimental accuracy when plotted as M/M_{sat} versus gB , where g is the g -factor appropriate for that direction of B (figure 1(c) and table 1). This suggests that the g -factor anisotropy is responsible for the observed angle dependence of B_c .

4. Monte Carlo simulations of magnetization data

The magnetic properties of the materials in table 1 are well described by $S = \frac{1}{2} \text{Cu}^{2+}$ spins on a square lattice. The layers are arranged in a tetragonal structure [18]; coupling between the layers

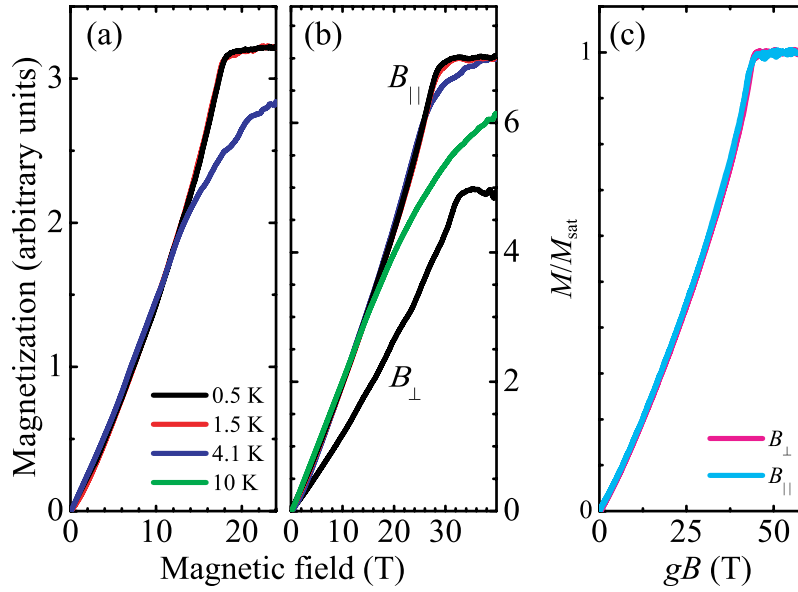


Figure 1. Pulsed-field magnetization data. (a) Magnetization M of $[\text{Cu}(\text{HF}_2)(\text{pyz})_2](\text{BF}_4)$ powder versus field B ; data for $T = 0.5, 1.5$ and 4.1 K are shown (traces for 0.5 and 1.5 K overlie). (b) Magnetization of $[\text{CuF}_2(\text{pyz})](\text{H}_2\text{O})_2$ single crystals with B applied parallel (upper 4 traces) and perpendicular (lower trace, 0.5 K) to the 2D planes. Data for $T = 0.5, 1.5, 4.1$ and 10 K are shown for the B_{\parallel} case. The ‘elbow’ denoting saturation occurs at $B_c = 28.8$ T for B_{\parallel} and $B_c = 33.1$ T for B_{\perp} . (c) Normalized M data ($T = 0.5$ K) for $[\text{Cu}(\text{HF}_2)(\text{pyz})_2]\text{ClO}_4$ single crystals versus gB , where g is the appropriate g -factor, for B parallel (B_{\parallel}) and perpendicular (B_{\perp}) to the 2D planes.

depends on the packing of the molecules between. To model data such as those in figure 1, we assume that the interaction between the spins is purely Heisenberg-like [1], resulting in the Hamiltonian

$$\mathcal{H} = J \sum_{\langle i,j \rangle_{xy}} \mathbf{S}_i \cdot \mathbf{S}_j + J_{\perp} \sum_{\langle i,j \rangle_z} \mathbf{S}_i \cdot \mathbf{S}_j - h \sum_i S_i^z, \quad (1)$$

where J (J_{\perp}) is the strength of the intra- (inter-) planar coupling and $h = g\mu_B B$ is the Zeeman energy provided by the (uniform) magnetic induction B . The first (second) summation refers to summing over all nearest-neighbors parallel (perpendicular) to the 2D xy -plane. The dependence of M as a function of B is studied for a range of values of J_{\perp}/J (from $J_{\perp} = 0$ (completely decoupled layers) to $J_{\perp}/J = 1$) using large-scale numerical simulations. Note that the orientation of B only affects h through the anisotropy of the g -factor, in agreement with the discussion of figure 1(c) above.

The stochastic series expansion (SSE) method [33]–[35] is a finite- T quantum Monte Carlo (QMC) technique based on importance sampling of the diagonal matrix elements of the density matrix $e^{-\beta\mathcal{H}}$, where the inverse T is represented by β , and \mathcal{H} is given by equation (1). Using the ‘operator-loop’ cluster update [34], the autocorrelation time for system sizes considered here (up to $\approx 3 \times 10^4$ spins) is at most a few Monte Carlo sweeps even at the critical T [37] for the onset of magnetic order. Estimates of ground state observables are obtained by using

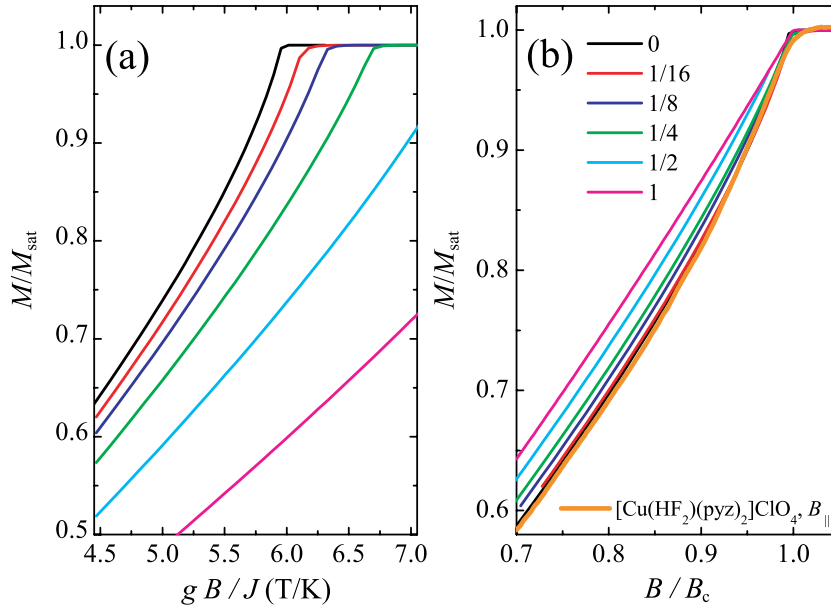


Figure 2. Comparison of model and data. (a) Calculated magnetization M of a spin- $\frac{1}{2}$ square lattice with added interlayer anisotropy (see equation (1)). Simulations are shown for $J_{\perp}/J = 0$ (uppermost curve) $\frac{1}{16}$, $\frac{1}{8}$, $\frac{1}{4}$, $\frac{1}{2}$ and 1 (lowest curve). Increasing J_{\perp}/J raises the critical field for saturation B_c and reduces the curvature of $M(B)$ below B_c . (b) Comparison of the model shown in (a) with experimental data (orange curve) for a $[\text{Cu}(\text{HF}_2)(\text{pyz})_2]\text{ClO}_4$ crystal ($T = 0.5$ K, field applied parallel to the 2D planes). Both model and data are plotted in reduced units M/M_{sat} and B/B_c . Note that the experimental data lie between the $J_{\perp}/J = 0$ and $J_{\perp}/J = \frac{1}{16}$ model curves.

sufficiently large values of β . We have further found that the statistics of the data obtained can be significantly improved by the use of a tempering scheme [37]–[39]. We use parallel tempering [38, 39], where simulations are run simultaneously on a parallel computer, using a fixed value of J_{\perp} and different, but closely spaced, values of $h = g\mu_B B$ over the entire range of fields up to saturation. Along with the usual Monte Carlo updates, we attempt to swap the values of fields for SSE configurations (processes) with adjacent values of h at regular intervals (typically after every Monte Carlo step, each time attempting several hundred swaps) according to a scheme that maintains detailed balance in the space of the parallel simulations. This has favorable effects on the simulation dynamics, and reduces the overall statistical errors (at the cost of introducing correlations between the errors, of minor significance here). Implementation of tempering schemes in the context of the SSE method is discussed in [40].

5. Comparisons of model and data

Figure 2(a) shows the predictions of the model for low T , and figure 2(b) shows a comparison with typical experimental data. This is made by plotting both model results and experimental data in dimensionless units, M/M_{sat} and B/B_c . As M_{sat} is known, there is in effect only one variable parameter, B_c . The value of B_c is varied until there is a satisfactory overlap of the data

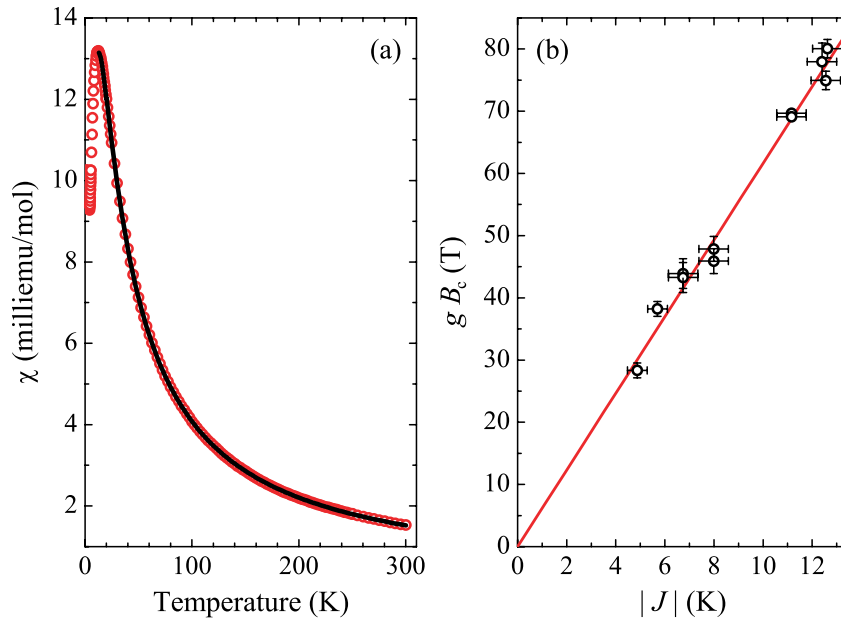


Figure 3. Comparing the model prediction with susceptibility data. (a) Temperature dependence of the low-field susceptibility χ of $[\text{Cu}(\text{HF})_2(\text{pyz})_2]\text{SbF}_6$ (points) fitted to the 2D Heisenberg expression (curve) of [41]⁹ to obtain an estimate of J . (b) Experimental saturation fields times g -factor (gB_c) plotted against values of J deduced using fits such as that in (a) (points). The straight-line fit to the data yields $gB_c/|J| = 6.2 \pm 0.2 \text{ T K}^{-1}$.

and one of the model curves. The curvature of the data and the presence of the ‘elbow’ place tight constraints on the comparison of data and model allowing B_c and the anisotropy J_\perp/J to be determined accurately. The comparison in figure 2(b) is typical of all of the materials in table 1, with their $M(B)$ data falling between, or closest to, the $J_\perp/J = 0$ or $J_\perp/J = \frac{1}{16}$ numerical curves, indicating a high degree of anisotropy. We shall give further justification for this assertion below.

From equation (1) it is seen that $g\mu_B B_c = 4J + 2J_\perp$, and so for such highly anisotropic magnets the model predicts the ratio $gB_c/|J|$ to take values in the range from 5.95 T K^{-1} ($J_\perp = 0$) to 6.10 T K^{-1} ($J_\perp/J = \frac{1}{16}$). Since the experimental uncertainties involved in the location of B_c are $\sim 1\text{--}2\%$, and the errors in g are $\sim 1\%$, no significant loss in accuracy occurs if we employ the mean value,

$$\frac{gB_c}{|J|} \approx 6.03 \text{ T K}^{-1}, \quad (2)$$

in what follows. To check the model prediction, a fit of the T -dependent low-field susceptibility following the method of [41]⁹ was used to determine J independently for a selection of compounds (figure 3(a)); the values obtained are compared with gB_c in figure 3(b)¹⁰. As can be seen, the points lie close to the line $gB_c/|J| = 6.2 \pm 0.2 \text{ T K}^{-1}$, in good agreement with the predicted value (equation (2)). As noted above, it is possible to determine the value of

⁹ Note the definition of J used in [41] differs by a factor of 2 from the one employed in the present paper.

¹⁰ An alternative expression that allows fitting of the susceptibility to lower temperatures is found in [26]. For the data in figure 3, the results obtained from both expressions are in excellent agreement.

B_c to a very good accuracy ($\pm 1-2\%$); once the dimensionality of the magnet in question is seen to fall within the limits $J_{\perp}/J \approx 0 - \frac{1}{16}$ using comparisons such as those in figure 2(b), equation (2) almost certainly presents the most accurate method for evaluating J . Intralayer exchange energies J derived in this way from measured values of g and B_c are in table 1.

Thus, we have developed a method for determining both J and T_N in anisotropic magnetic systems. In addition, an estimate of the anisotropy $|J_{\perp}/J|$ can be made using the results of quantum Monte Carlo simulations of quasi-2D Heisenberg antiferromagnets [42]. This study found

$$\frac{|J_{\perp}|}{|J|} = \exp\left(2.43 - 2.30 \times \frac{|J|}{T_N}\right), \quad (3)$$

where both $|J|$ and T_N are measured in K; the resulting values are given in table 1. Note that equation (3) is a rapidly varying function of $|J|/T_N$; small shifts in either parameter result in quite large changes in $|J_{\perp}/J|$. Given the experimental and other errors in J and T_N (\sim a few %), the derived values of $|J_{\perp}/J|$ will probably be within a factor ~ 2 of the true values. In spite of this caveat, the $|J_{\perp}/J|$ values in table 1 are all $\lesssim 0.01$, in good agreement with the comparison of the model and the magnetization data (e.g. figure 2) that suggested $0 \lesssim |J_{\perp}/J| \lesssim \frac{1}{16}$ for all of the compounds.

6. Systematic trends in the $[\text{Cu}(\text{HF}_2)(\text{pyz})_2]\text{X}$ family

Having established a reliable method for deriving J and the anisotropy from $M(B)$ and T_N , we focus our remaining discussion on the compounds with formula $[\text{Cu}(\text{HF}_2)(\text{pyz})_2]\text{X}$, ([18], footnote 8) where X can be ClO_4 , BF_4 , PF_6 , etc (table 1). All of these materials possess very similar extended polymeric structures consisting of 2D, four-fold symmetric $[\text{Cu}(\text{pyz})_2]^{2+}$ sheets in the ab -planes that are connected along the c -axis by linearly bridging HF_2 groups (figure 4) ([18], footnote 8). The Cu–Cu separations are similar along the Cu–(pyz)–Cu and Cu–FHF–Cu (e.g. 0.6852 and 0.6619 nm, respectively, for X = BF_4 at room temperature) linkages, so that the structure may be described as pseudo-cubic ([18], footnote 8); the X counterions are placed in the body-center positions within each ‘cube’. The Cu–F and Cu–(pyz) bonds result in the $\text{Cu}^{2+} d_{x^2-y^2}$ orbitals lying within the ab -planes, as evidenced by the g -factor anisotropy observed in EPR measurements (table 1); as noted above, the ab -planes also correspond to the 2D planes within which the strong exchange pathways occur.

There is little variation of the in-plane Cu–Cu distance across the $[\text{Cu}(\text{HF}_2)(\text{pyz})_2]\text{X}$ series ([18], footnote 8); given this similarity, it is at first sight surprising that the in-plane exchange parameters J in table 1 fall into two distinct groups: the compounds with tetrahedral counterions (X = BF_4 and ClO_4) possess values $J \approx -7$ K and those with octahedral counterions (X = PF_6 , SbF_6 and AsF_6) have $J \approx -13$ K. Note also that the compounds with tetrahedral counterions are more anisotropic ($|J_{\perp}/J| \sim 10^{-3}$) than those with octahedral counterions ($|J_{\perp}/J| \sim 10^{-2}$).

We now discuss whether the non-coordinating X counterions can play a direct role as exchange pathways between the Cu^{2+} ions. First of all, the molecules ClO_4 and BF_4 have radically different electronic orbitals, and yet the in-plane exchange energies for the magnets containing these counterions are very similar (see the first three rows of table 1). Moreover, as mentioned above, the X counterions are not within the 2D Cu^{2+} planes, but at body-center positions within the ‘cubes’ (figure 4). The Cu–X separation is therefore roughly the same for

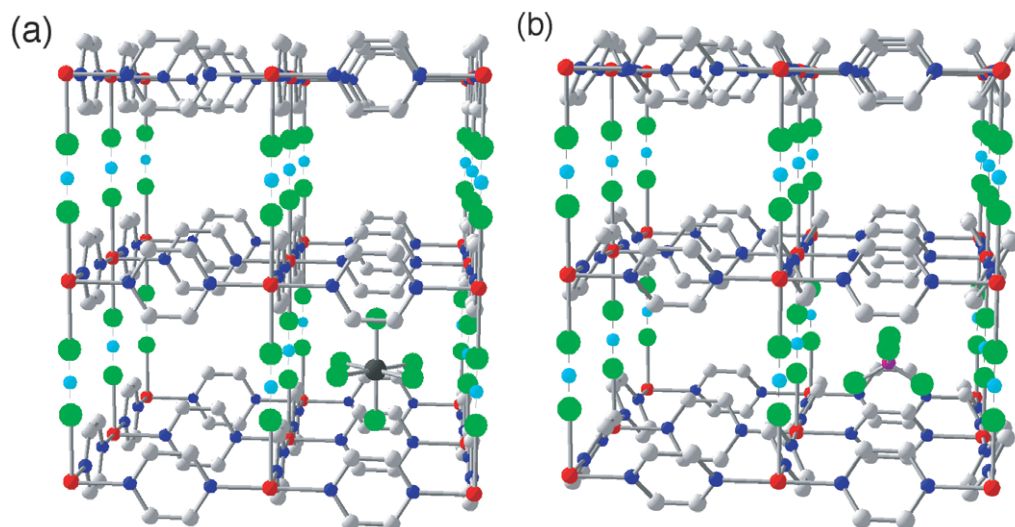


Figure 4. Experimentally determined ([18], footnote 8) room temperature crystal structures of $[\text{Cu}(\text{HF}_2)(\text{pyz})_2]\text{X}$ 2D metal-organic magnets. (a) $\text{X} = \text{SbF}_6$; (b) $\text{X} = \text{BF}_4$. The Cu ions (red) are bridged by organic pyrazine ligands within the ab -planes in which the strong exchange pathways occur. These magnetic layers are separated by HF_2 bridging groups. The non-coordinating $[\text{SbF}_6]^-$ and $[\text{BF}_6]^-$ counterions inhabit the ‘body-center’ sites of each approximately cubic unit; in all but one of the cubic units in (a) and (b) they have been omitted for clarity. Note that for $\text{X} = \text{BF}_4$ (b), the planes of the pyrazine molecules are tilted by 31.6° away from being orthogonal to the magnetic layers. However, for $\text{X} = \text{SbF}_6$ (a), the tilt angle is rather smaller (0° at room temperature). Cu = red, F = green, N = blue, C = gray, H = cyan, Sb = black and B = purple. Hydrogen bonds are shown as dotted lines.

the in-plane and inter-plane directions; if the X counterions played a direct role as exchange pathways, one might expect that the $[\text{Cu}(\text{HF}_2)(\text{pyz})_2]\text{X}$ compounds would have $|J_\perp/J|$ values that were somewhat larger (i.e. more isotropic) than the values $\sim 10^{-3}$ – 10^{-2} that are actually observed (see table 1). Therefore, instead of playing a direct role in the exchange, it is more likely that it is an counterion *size effect* on the crystal structure that is affecting the exchange pathways. The size of the counterion in the direction perpendicular to the planes differs by a factor of approximately 2 at room temperature for the tetrahedral and octahedral counterions (see footnote 8 and figure 4). This leads to a modest change in the respective interlayer Cu–Cu distances, d_\perp . For example, there is a $\sim 5\%$ difference between the $\text{X} = \text{BF}_6$ ($d_\perp \approx 6.62 \text{ \AA}$) and the $\text{X} = \text{SbF}_6$ ($d_\perp \approx 6.95 \text{ \AA}$) compounds (see footnote 8). This trend in inter-plane distance is opposite to that might be expected given that J_\perp appears to be enhanced in the compounds with octahedral counterions (see table 1), and it certainly cannot by itself account for the large change in the in-plane exchange energy.

The structural difference that may be well responsible for the factor of two change in J is the configuration of the pyz molecules within the Cu–(pyz)–Cu linkages. Figure 4 (upper) shows $[\text{Cu}(\text{HF}_2)(\text{pyz})_2]\text{SbF}_6$, one of the systems with octahedral counterions; the structures of $\text{X} = \text{AsF}_6$, PF_6 are very similar. At room temperature, geometry of the octahedral counterions allows the pyz ligands to stand up virtually perpendicular to the ab planes (see footnote 8

and figure 4). By contrast, the planes of the pyz ligands in the compounds with the smaller tetrahedral counterions, $[\text{Cu}(\text{HF})_2(\text{pyz})_2]\text{BF}_4$ (figure 4 (lowest)) and $[\text{Cu}(\text{HF})_2(\text{pyz})_2]\text{ClO}_4$, are not perpendicular to the ab -planes, but are tilted away by 31.6° ($X = \text{BF}_4$) or 25.8° ($X = \text{ClO}_4$) in a pattern that preserves the four-fold symmetry of the Cu^{2+} sites (see footnote 8). This suggests that it may be the orientation dependence of the pyz ligand that produces the factor of two differences in J , with the more perpendicularly disposed pyzs (figure 4) presenting a more efficient exchange pathway within the layers.

Although we cannot rule out the possibility of a structural distortion occurring in these compounds as the temperature is reduced, EPR measurements show no evidence for changes in the local symmetry of the magnetic Cu^{2+} ion on cooling to T_N . Therefore, at present it seems unlikely that any such structural reorientation could lead to the observed disparity between the compounds with counterions of different symmetries.

7. Summary

Magnetization experiments have been carried out on nine metal–organic Cu-based 2D Heisenberg magnets. These systems exhibit a low- T magnetization that is concave as a function of field, with a sharp ‘elbow’ transition to a constant saturation value at a critical field B_c . Monte Carlo simulations including interlayer exchange quantitatively reproduce the data; the concavity indicates the effective dimensionality and B_c is an accurate measure of the in-plane exchange energy J . Taken in conjunction with Néel temperatures derived from μSR , the values of J may be used to obtain quantitative estimates of the exchange anisotropy, $|J_\perp/J|$.

We suggest that in metal–organic magnets of the form $[\text{Cu}(\text{HF}_2)(\text{pyz})_2]\text{X}$, where X is a non-coordinating counterion molecule, the sizes of J and J_\perp may be controlled by the tilting of the pyz molecule with respect to the 2D planes. Thus, it may be possible to use molecular architecture to design magnets with very specific values of J , tailored to a particular desired property.

Another way of looking at these structures is that they are pseudo-perovskite ABL_3 , where the A is the counterion (BF_4 , ClO_4 , etc), Cu is the B cation and L are the coordinated bridges, pyz and HF_2 . In light of this, one possible application would be a metal–organic magnet designed to simulate the antiferromagnetic interactions germane to cuprate superconductivity [3], [10]–[14], but with exchange energies small enough to permit manipulation of the magnetic groundstate using standard laboratory fields.

Acknowledgments

We thank Peter Baker and Alex Amato for experimental assistance and Bill Hayes for stimulating discussions. This work was supported by the US Department of Energy (DoE) BES program ‘Science in 100 T’. Work at NHMFL is performed under the auspices of the National Science Foundation, the DoE and the State of Florida. Work at Argonne is supported by the Office of Basic Energy Sciences, DoE (contract DE-AC02-06CH11357). Part of this work was carried out at the Swiss Muon Source, Paul Scherrer Institut, Villigen, Switzerland, and at the ISIS Facility, Rutherford-Appleton Laboratory, UK. Work carried out at EWU was supported by an award from the Research Corporation. TL, PAG and SC acknowledge support from the Royal Commission for the Exhibition of 1851, the Glasstone Foundation and the Seaborg Institute, respectively. JS thanks Oxford University for the provision of a Visiting Professorship.

References

- [1] Kastner M A, Birgeneau R J, Shirane G and Endoh Y 1998 *Rev. Mod. Phys.* **70** 897
- [2] Schollwöck U, Richter J, Farnell D J J and Bishop R F (ed) 2004 *Quantum Magnetism* (Berlin: Springer)
- [3] Manousakis E 1991 *Rev. Mod. Phys.* **53** 1
- [4] Christensen N B *et al* 2007 *Proc. Natl Acad. Sci. USA* **104** 15264
- [5] Vajk O P, Mang P K, Greven M, Gehring P M and Lynn J W 2002 *Science* **295** 1691
- [6] Deng D S, Jin X F and Tao T 2002 *Phys. Rev. B* **65** 132406
- [7] Beard BB, Cuccoli A, Vaia R and Verrucchi P 2003 *Phys. Rev. B* **68** 104406
- [8] Sengupta P, Sandvik A W and Singh R R P 2003 *Phys. Rev. B* **68** 094423
- [9] Zhang R and Zhu S Q 2006 *Phys. Lett. A* **348** 110
- [10] Schrieffer J R and Brooks J S (ed) 2007 *High Temperature Superconductivity Theory and Experiment* (Berlin: Springer)
- [11] Dai P, Mook H A, Hunt R D and Doğan F 2001 *Phys. Rev. B* **63** 054525
- [12] Stock C *et al* 2005 *Phys. Rev. B* **71** 024522
- [13] Julian S R and Norman M 2007 *Nature* **447** 537
- [14] Harrison N, McDonald R D and Singleton J 2007 *Preprint* 0710.1932
- [15] Monthoux P, Pines D and Lonzarich G G 2007 *Nature* **450** 1177
- [16] Mermin N D and Wagner H 1966 *Phys. Rev. Lett.* **17** 1133
- [17] Choi J, Woodward J D, Musfeldt J L, Landee C P and Turnbull M M 2003 *Chem. Mater.* **15** 2797
- [18] Manson J L *et al* 2006 *Chem. Commun.* 4894
- [19] Lancaster T *et al* 2007 *Phys. Rev. B* **75** 094421
- [20] Deumel M, Landee C P, Novoa J J, Robb M A and Turnbull M M 2003 *Polyhedron* **22** 2235
- [21] Lancaster T *et al* 2006 *Phys. Rev. B* **73** 020410
- [22] Blundell S J *et al* 2007 *J. Phys. Chem. Solids* **68** 2039
- [23] Manson J L *et al* 2008 *Chem. Mater.* submitted
- [24] Goddard P A *et al* 2008 *Preprint* 0807.1506
- [25] Abragam A and Bleaney B 1970 *Electron Paramagnetic Resonance of Transition Ions* (Oxford: Oxford University Press) p 208
- [26] Woodward F M *et al* 2007 *Inorg. Chem.* **46** 4256
- [27] Lancaster T *et al* 2007 *Phys. Rev. Lett.* **99** 267601
- [28] Cox S, McDonald R D, Funk K, Southerland H A, Manson J L and Schlueter J A 2008 in preparation
- [29] Poole C P Jr 1982 *Electron Spin Resonance: A Comprehensive Treatise on Experimental Techniques* (New York: Wiley)
- [30] Goddard P A *et al* 2007 *Phys. Rev. B* **75** 094426
- [31] Detwiler J A *et al* 2000 *Phys. Rev. B* **61** 402
- [32] Jaime M, Lacerda A, Takano Y and Boebinger G S 2006 *J. Phys.: Conf. Ser.* **51** 643
- [33] Sandvik A W and Kurkijärvi 1991 *Phys. Rev. B* **43** 5950
- [34] Sandvik A W 1997 *Phys. Rev. B* **56** 11678
- [35] Sandvik A W 1999 *Phys. Rev. B* **59** 14157
- [36] Syljuåsen O F and Sandvik A W 2002 *Phys. Rev. E* **66** 046701
- [37] Marinari E 1998 *Adv. Comput. Simul.* **501** 15
- [38] Hukushima K, Takayama H and Nemoto K 1996 *Int. J. Mod. Phys. C* **7** 337
- [39] Hukushima K and Nemoto K 1996 *J. Phys. Soc. Japan* **65** 1604
- [40] Sengupta P, Sandvik A W and Campbell D K 2002 *Phys. Rev. B* **65** 155113
- [41] Landee C P, Roberts S A and Willett R D 1978 *J. Chem. Phys.* **68** 4574
- [42] Yasuda C *et al* 2005 *Phys. Rev. Lett.* **94** 217201